RESEARCH ARTICLE

Direct Arm Energy Control of the Modular Multilevel Matrix Converter

MILAN UTVIĆ, (Graduate Student Member, IEEE),
PHILIPPE BONTEMPS, (Graduate Student Member, IEEE),
AND DRAŽEN DUJIĆ, (Senior Member, IEEE)

Power Electronics Laboratory, École Polytechnique Fédérale de Lausanne (EPFL), 1015 Lausanne, Switzerland

Corresponding author: Philippe Bontemps (philippe.bontemps@epfl.ch)

ABSTRACT Modular multilevel matrix converter is a type of converter used in medium-voltage ac-ac power conversion. Controlling the energy content of the converter arms is a prerequisite for a proper converter operation, and at the same time a challenging control task. So far, there are several approaches presented in the literature that successfully deal with the challenge. However, almost all of them fail when it comes to the simplicity of implementation, and ease of understanding by control engineers and researchers entering the field. This paper extends the direct arm energy control concept, already introduced for the class of modular multilevel converters, to the modular multilevel matrix converter. Presented control approach is characterized by an intuitive and simple implementation, ability to control the arm energies to arbitrary values, and stable operation under all operating conditions, including grid imbalances. Validity of the control concept was demonstrated using an in-house-developed hardware-in-the-loop simulator of the modular multilevel matrix converter, with control algorithms being deployed to the industrial-grade controller.

INDEX TERMS Modular multilevel converter, modular multilevel matrix converter, energy control, hardware-in-the-loop, ac-ac power conversion.

I. INTRODUCTION

The modular multilevel matrix converter (M3C) was firstly introduced without arm inductors [1], similar to the standard modular multilevel converter (MMC) [2], which initially followed the same approach. Absence of the arm inductors imposed limitations on the number of switching states due to the associated risks of inter-arm short circuits, so later publications almost exclusively employed arm inductors. This converter topology is used for medium-voltage ac-ac conversion tasks, typically for interfacing two three-phase (3PH) systems, or a 3PH and a single-phase (1PH) system, though it can be used to interface multiphase systems as well. It is applied in railway interties [3], where it connects a 3PH utility grid with a 1PH medium voltage (MV) railway grid,

The associate editor coordinating the review of this manuscript and approving it for publication was Branislav Hredzak.

typically with a different frequency. Main benefits compared to the standard solutions, e.g with three-level NPC converters, are a possibility of elimination of a bulky transformer on the railway side, increased reliability, and elimination of the second-harmonic filter [4]. In general, the M3C can be also applied in MV motor drives, especially in low-speed drives with a constant torque characteristic [5], as well as with variable-speed synchronous machines in pumped-hydro storage power plants [6].

High reliability achieved through redundancy, high efficiency, elimination of bulky filters and transformers come with the price of increased control complexity. One of the control challenges is to ensure that the energy content within each arm of the converter corresponds to its reference. In addition, it is necessary to equally distribute the energy content among the submodules (SM) of an arm, which is accomplished using different control techniques

[2], [7], [8], [9]. Nevertheless, those control actions are completely decoupled from the arm energy control, and will not be discussed within this paper.

Reference [10] presents a generalized set of criteria for the arm energy balancing, applicable to different MMC-alike topologies, such as the standard MMC, delta and star STATCOM, matrix MMC and Hexverter. Although the stability of the method has been confirmed by means of simulation, using the M3C as an example, this reference only mathematically formulates the criteria, and does not present a solution for any particular converter, neither does it provide guidelines for the implementation. In [11] authors use the approach from [10] to balance the energies inside a standard MMC converter, demonstrating that the application of this method requires a profound mathematical expertise in obtaining a solution.

The first references successfully dealing with this topic [12], [13] propose a set of solutions for the M3C energy control, based on circulating currents and common-mode voltage injection, which might be used in different ways, depending on the operating mode. While it demonstrates the ability to create an arbitrary imbalance among the converter arms, implementation of this method is based on double-$\alpha\beta0$ transformations, which might not be an intuitive approach and requires a considerable amount of direct and inverse double-$\alpha\beta0$ transformations. Similar approach was used in [14], where the authors experimentally demonstrate the effectiveness of the balancing method. Apart from a significant amount of double-$\alpha\beta0$ transformations, validity of the method was not tested under unbalanced grid conditions.

Improvement of the method presented in [13] was proposed in [15], where an additional $\Sigma\Delta$ transformation is performed on the internal $\alpha\alpha, \alpha\beta, \beta\alpha, \beta\beta$ currents, in order to decouple specific frequency components. The same approach was used by the authors in [16] and [17], which use the M3C as an interface between the wind generator and the ac utility grid. While this approach reduces the delay of the filtering chain in each of the specific directions, the overall delay is determined by the slowest among them. As a result, no significant benefits are expected in terms of control dynamics, while the realization of the control method gets even more complicated. In addition, relationship between the controlled current components in diagonal directions and the final arm currents become even more complex, which makes it difficult to both understand and limit the influence of a certain control action on a particular arm current.

Authors in [18] present a generalized approach for current control and energy balancing, applicable to any of the modular multilevel converter topologies. The approach is based on using circulating current components at both the grid and the load frequency, as well as common-mode voltages and circulating current components at arbitrary frequencies. The optimal solutions, in terms of minimal RMS of the induced circulating currents, were presented in the form of matrices, which yield circulating current and common-mode voltage references from the arm power references. Two matrices are presented, where each one of them is optimal for different operating ranges of the M3C. While the solution poses lower current stress on the converter for some operating points compared to [14], the implementation of the method is not simple, due to the fact that the resulting matrices are of high order, and the elements of the matrix are variables dependent upon the operating condition, which are calculated in real time. High number of different elements in the matrices that are either used as inputs or calculated in real-time increases the risk of an error during implementation of the method. In addition, a clear distinction between the application range of the two methods has not be presented, which could lead to a transient behaviour of the converter during the hard switchover between the two. Applicability of the method was not tested under unbalanced grid conditions. Although the proposal combines all degrees of freedom and yields an effective solution with the minimal current stress, its lack of simplicity of implementation might render it unattractive, particularly for engineers and researchers entering the field.

Recent publications on this topic [19], [20], [21] address the energy control issue in the M3C by searching for an optimal combination of the circulating currents and a common-mode voltage based on the model-predictive control principles. Fundamentally, all these methods are based on double-$\alpha\beta0$ modeling of the converter, while the model-predictive control serves to find the most optimal solution. While all of them manage to find an optimal combination between the circulating currents and the common-mode voltage, these solutions are in the authors opinion quite complex for implementation. Besides multiple double-$\alpha\beta0$ and inverse double-$\alpha\beta0$ transformations, calculation of the optimal circulating currents involves the use of dynamic calculation of the optimal matrix coefficients. Even though the authors claim that these optimization problems can be resolved offline, they still require a thorough offline analysis for all operating points, and feeding the optimal coefficients for all operating points into the look-up tables. All these analyses become even more complex when unbalanced grid conditions, arbitrary energy references, and arbitrary common-mode voltage amplitudes come into play.

Complexity of the existing solutions for the M3C energy control was recognized by the authors in [22], who proposed an energy balancing solution that simplifies the energy control problem in the M3C, compared to the existing solutions. Although effectively achieving the balancing task within the converter under symmetrical conditions, proposed solution is unable to deal with the energy control in cases when different energy levels are required in different arms (as in the case of a SM failure in one arm). In addition, the solution might not be able to ensure the decoupling of the inner energy control from the terminal currents during grid faults.

Another issue with operation of the M3C arises when the frequencies of the two ac system it interconnects become similar or equal. In such a case, energy oscillations in the M3C arms become excessively high, resulting in a large ripple in the voltage of the arm capacitors. If not mitigated, excessively high voltage ripple would lead to overvoltages across

SM capacitors, loss of the voltage generation capability, and consequently loss of control over the converter. Mitigation of such oscillations relies on introduction of a common-mode voltage and circulating currents, which together counteract the power components that provoke the oscillations [14], [15], [17], [23], [24], [25]. Regardless of the control method being applied, what all of them have in common is the fact that the arm current increases significantly due to the introduced circulating currents. It can go up to 50% above the rated arm current [5], [26]. Additionally, voltage oscillations in case when the supply and load frequencies are equal are still 2.5 times higher in case of the M3C compared to the back-to-back MMC solution, yielding a requirement for a higher installed energy in the M3C. All this facts contribute to the conclusion that the M3C is a converter suitable for interconnecting two ac systems of unequal frequencies, or an ac motor drive with a rated frequency far below the supply frequency. Therefore, the focus of the paper is on techniques for the arm energy control in the M3C, assuming that the frequencies of the interconnected systems are sufficiently different from each other.

This paper presents an extension of the direct arm energy control methods, firstly derived for a standard MMC [27], [28], to the M3C. The methods presented within this paper are characterized by an intuitive and simple implementation, which might be of great value to the control engineers and researchers entering the field. In addition, it is able to independently control arm energies to arbitrary values, and is also valid under balanced and unbalanced grid conditions. Control methods presented in this papers are deployed to the industrial-grade controller, and verified on an in-house-developed hardware-in-the-loop (HIL) simulator of the M3C converter. The case of variable-speed drive is used as a test case.

Section II presents the basic equations and operating principles behind the M3C. Derivation of the methods for direct arm energy control, originally developed for the standard MMC, are presented in Section III, whereas their extension to the M3C was presented in Section IV. Description of the real-time (RT) hardware-in-the-loop (HIL) simulator used for the control verification is given in Section V, whereas the results of the RT HIL simulations are provided in Section VI, while a brief discussion of the results is provided in Section VII. Finally, conclusions of the paper are outlined in Section VIII.

II. MODELLING OF THE M3C

Electrical schematic of an M3C is provided in Fig. 1. It interfaces a 3PH ac grid, characterized by its phase voltages v_A, v_B, and v_C, with another 3PH grid/load, that can represent a 3PH ac machine. Without loss of generality, the terminals labelled as ABC will be further referred to as grid terminals, whereas the terminals labelled with 123 will be further referred to as load terminals.

Each grid terminal of an M3C is connected with each load terminal via a dedicated arm. Arm is a cluster of FB SMs connected in series, together with an arm inductor, which

permits arm current control. Under normal operating conditions, a cluster of SMs can be perceived as a controllable voltage source, which can generate an arbitrary multilevel voltage waveform. Therefore, for the sake of analysis of the terminal currents and voltages, we will assume that the clusters of SMs are acting as ideal voltage sources.

Due to the symmetry among the arms, only a single arm will be considered during the following analysis. Applying a Kirchoff's law to the arm interfacing the terminals A and 1, yields:

$$L_{arm} \frac{di_{A1}}{dt} = v_A - v_{A1} - v_1 - v_{comm} \quad (1)$$

Since an arm interconnects a grid-side and load-side terminal, it will contain portion of both terminal currents. Additional arm current components at grid and load frequency might be injected to perform the arm energy control, labelled as Δi_{A1} and δi_{A1}, respectively. The arm voltage comprises terminal voltage components, as well as current control components, as shown in (3). Equation (4) shows that all the arm current components can be fully controlled by the arm voltage components. Consequently, terminal currents can be independently controlled, and decoupling between the two systems can be fully achieved.

$$i_{A1} = i_{A1}^{(\omega_g)} + i_{A1}^{(\omega_l)} + \Delta i_{A1} + \delta i_{A1} \quad (2)$$

$$v_{A1} = v_A - v_1 - v_{comm} - \Delta v_A - \Delta v_1 - \Delta v_\Delta - \Delta v_\delta \quad (3)$$

$$L_{arm} \frac{d}{dt} \left(i_{A1}^{(\omega_g)} + i_{A1}^{(\omega_l)} + \Delta i_{A1} + \delta i_{A1} \right)$$
$$= \Delta v_A + \Delta v_1 + \Delta v_\Delta + \Delta v_\delta \quad (4)$$

The total voltage across the SM capacitors inside an arm is a reflection of the total energy stored within these capacitors. The energy content is controlled by the arm power, which can be expressed as in (5). Contribution of the voltage components Δv_A, Δv_1, Δv_Δ, and Δv_δ which are normally very small compared to the other voltage components in (3), is neglected.

$$p_{A1} = v_{A1} i_{A1} = (i_{A1}^{(\omega_g)} + i_{A1}^{(\omega_l)} + \Delta i_{A1} + \delta i_{A1})$$
$$\times (v_A - v_1 - v_{comm}) \quad (5)$$

References [5] and [23] demonstrate that the M3C is a preferable solution for interconnecting low-speed, high-torque drives to the medium-voltage grid, or generally to interface two systems with different operating frequencies. Consequently, the two systems of unequal frequencies will be considered here. Arm power components can have non-zero average values over their periods only in case when the voltage and current component are of equal frequencies. To analyse the arm power components, the following definition of the quantities from (5) is adopted:

$$v_A = \hat{V}_A \cos(\omega_g t) \quad (6)$$

$$v_1 = \hat{V}_1 \cos(\omega_l t + \Theta_l) \quad (7)$$

$$i_{A1}^{(\omega_g)} = \hat{I}_{A1}^{(\omega_g)} \cos(\omega_g t - \phi_g) \quad (8)$$

$$i_{A1}^{(\omega_l)} = \hat{I}_{A1}^{(\omega_l)} \cos(\omega_l t + \Theta_l - \phi_l) \quad (9)$$
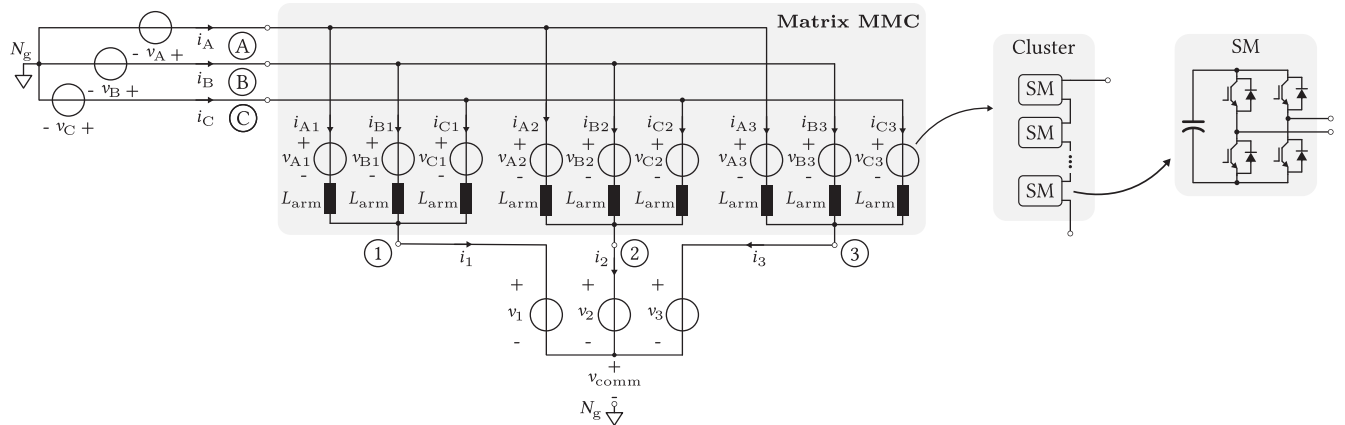
FIGURE 1. Topology of an M3C converter. The M3C interfaces two 3PH ac grids in general case. Every terminal of one grid is connected to a terminal of the other grid through a dedicated arm. The arm consists of a cluster of SMs in series with an arm inductor. SMs are of full-bridge (FB) type, so to be able to generate voltages of both polarity.

$$\Delta i_{A1} = \Delta \hat{I}_{A1} \cos(\omega_g t - \phi_{\Delta g}) \tag{10}$$

$$\delta i_{A1} = \delta \hat{I}_{A1} \cos(\omega_l t - \phi_{\Delta l}) \tag{11}$$

$$v_{comm} = \hat{V}_{comm}^{(\omega_g)} \cos(\omega_g t + \Theta_{comm,g})$$
$$+ \hat{V}_{comm}^{(\omega_l)} \cos(\omega_l t + \Theta_{comm,l}) \tag{12}$$

The additional arm current components, as well as common-mode voltage components are considered to be either at the grid or load frequencies, despite other different possibilities. The reason for such a choice is the fact that these components can interact with already present system variables (voltages and currents), and thus contribute to the arm energy control. As a result, injection of voltage and current components at another frequencies is avoided. Combining (6)-(12) into (5), and highlighting the components with non-zero average value gives the expression for the average arm power:

$$P_{A1} = \underbrace{\frac{\hat{V}_A \hat{I}_{A1}^{(\omega_g)} \cos \phi_g}{2}}_{P_{g,A1}} - \underbrace{\frac{\hat{V}_1 \hat{I}_{A1}^{(\omega_l)} \cos \phi_l}{2}}_{P_{l,A1}} + \dots$$

$$+ \underbrace{\frac{\Delta \hat{I}_{A1} \hat{V}_A \cos(\phi_{\Delta g})}{2}}_{P_{\Delta 1}} + \underbrace{\frac{\delta \hat{I}_{A1} \hat{V}_1 \cos(\phi_{\Delta l})}{2}}_{P_{\Delta 2}} + \dots$$

$$+ \underbrace{\frac{\hat{V}_{comm}^{(\omega_g)} \hat{I}_{A1}^{(\omega_g)} \cos(\phi_g + \Theta_{comm,g})}{2}}_{P_{\Delta 3}} + \dots$$

$$+ \underbrace{\frac{\hat{V}_{comm}^{(\omega_l)} \hat{I}_{A1}^{(\omega_l)} \cos(\phi_l + \Theta_{comm,l})}{2}}_{P_{\Delta 4}} \tag{13}$$

The first two terms in (13) represent the average power delivered to the arm from the grid and taken by the load, respectively. Another two power terms, $P_{\Delta 1}$ and $P_{\Delta 2}$, are a consequence of interaction between the additional arm current components at the grid and load frequency with the respective terminal voltages. The last two terms,

$P_{\Delta 3}$ and $P_{\Delta 4}$, are a consequence of interaction between the common-mode voltage components and the terminal currents.

Since only the first two terms in (13) normally exist in the average arm power, one might conclude that those two terms are sufficient to control the arm energy. Namely, by controlling either of the terminal current component, i.e. $\hat{I}_{A1}^{(\omega_g)}$ or $\hat{I}_{A1}^{(\omega_l)}$, one can control the arm power, and thus the arm energy content. However, due to different constraints, it is not possible to control the arm terminal currents independently which is the reason for the additional arm current and common-mode voltage injection.

III. ARM ENERGY CONTROL

To control energy content within each arm, a feedback-based approach is used. Arm energies are calculated from the measured SM voltages v_c as $W = C_{SM} \sum_{k=1}^{N} v_{c,k}^2 / 2$, and further filtered to exclude all harmonic components at the frequencies $2\omega_g$, $2\omega_l$, $(\omega_g + \omega_l)$, $(\omega_g - \omega_l)$, retaining only the dc values. Arm energy references are calculated based on desired SM voltages, as $W^* = N C_{SM} (V_c^*)^2 / 2$, where C_{SM} represents capacitance of a SM, whereas N denotes the number of SM within an arm. Nine PI controllers are used, to control the average energy content within each arm, giving the power references as their outputs.

Referring to the first two terms in (13), energy content within an arm can be controlled either by controlling the grid, or load current. For the sake of simplicity, it will be assumed that whenever in operation, the grid voltage is available, which does not necessarily hold for the load voltage. Therefore, the grid current can be used to maintain the energy content at desired value. Nevertheless, power requirements of energy controllers are in general arbitrary, and so would be the grid current requirements of individual arms, which would result in asymmetrical grid currents, as well as the appearance of the grid frequency currents in the load. To prevent such a scenario, arms are grouped into the bundles of three, where
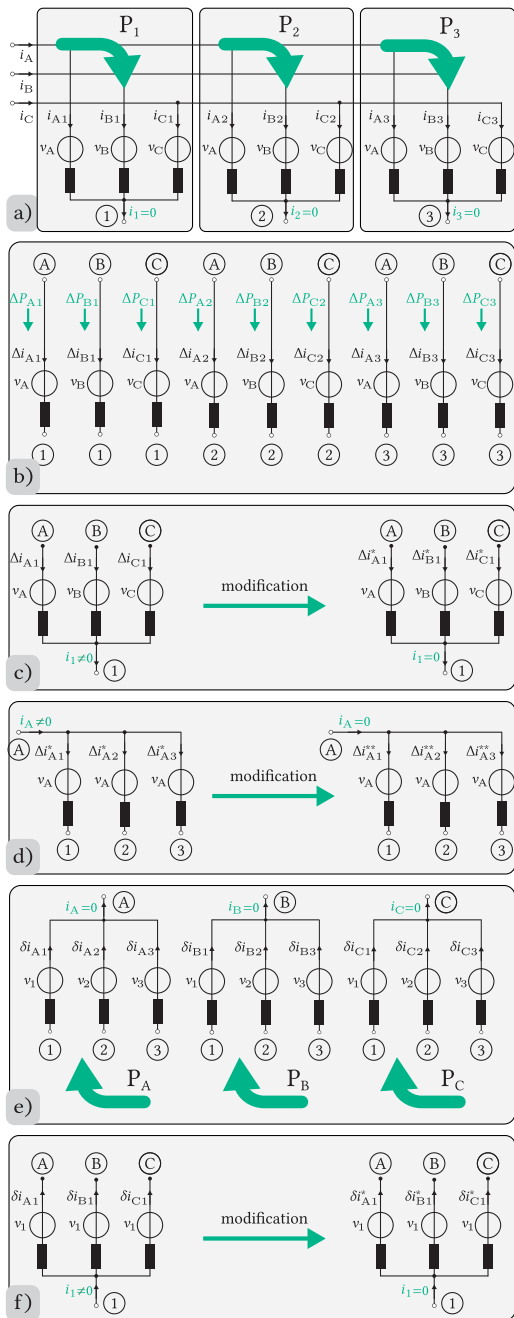
FIGURE 2. a) Grid current control for appropriate power distribution among the bundles of arms connected to the same load terminals; b) generation of additional arm current components Δi_{xy} at grid frequency, corresponding to the power requirements of individual arms ΔP_{xy}; c), d) illustration of the need for modification of the additional arm currents Δi_{xy} entering the same load/grid terminal; e) proper power distribution among the arm bundles connected to the same grid terminals through the additional arm currents at load frequency δi_{xy}; f) illustration of the need for modification of the additional load-frequency currents. Principles of the current modification are elaborated in Section IV.

each bundle represents arms connected to the same load terminal, as illustrated in Fig. 2.a. The total power requirement of a bundle equals the sum of power requirements of energy controllers (ΔP_{xy}) and the average power delivered to the

load through the respective node ($P_{\text{load},y}$):

$$P_y = \Delta P_{Ay} + \Delta P_{By} + \Delta P_{Cy} + P_{\text{load},y} \quad (14)$$

Thus obtained power reference can be realized using a set of symmetrical grid currents, and the positive sequence of the grid voltage. Resulting arm current components are calculated as in (15), where x refers to the grid terminals ABC, whereas y refers to the load terminals 123. This notation is used throughout the rest of the paper.

$$i_{xy}^{(\omega_g)} = \frac{2P_y}{3(V_g^+)^2} v_x^+ \quad (15)$$

Resulting current components do sum-up to zero at the load terminals, whereas their sum at the grid terminals corresponds to the total current drawn from the grid. Therefore, using the grid current components ensures that the power delivered to the three bundles corresponds to the total power references requested by the energy controllers within each bundle. However, nine arm energies have to be controlled, which calls for exploiting other degrees of freedom from (13).

Due to the assumption that the grid voltage is constantly available during the converter operation, using $P_{\Delta 1}$ power components from (13) seems to be the most reasonable choice. To create this power component within an arm, it is necessary to inject an additional arm current component at the grid frequency, as illustrated in Fig. 2.b. This current component should be in phase with the respective grid voltage, as it would results in a minimal current amplitude for a given power reference.

$$\Delta i_{xy} = \frac{2\Delta P_{xy}}{\hat{V}_x^2} v_x \quad (16)$$

Referring to Fig. 2.b, additional arm current references are generated in a way described by (16). Due to the arbitrary magnitude of these current references, as well as due to the asymmetrical system of grid voltages under unbalanced grid conditions, these currents do not generally sum-up to zero, and would appear in the load current, interfering with the load current controller. For such a reason, certain modification of the current references is required, to ensure that these currents sum-up to zero at the terminal 1, as illustrated in Fig. 2.c. One should also recall that these current references are generated in-phase with its respective grid voltages, so as to minimize their magnitude. Therefore, the modification imposed on these currents should be such that, apart from the zero-sum condition, the deviation from the original references is minimized, thus obtaining a set of currents that impose the minimal thermal stress on the converter arms.

In addition to not being observed at the load terminals, these additional current components should neither be observed at the grid terminals. This condition is shown in Fig. 2.d, where the arms connected to the same grid terminals are grouped. Previously modified current references Δi_{xy}^* are further modified so that they sum-up to zero, and thus remain unobserved at both converter terminals. Current modification,

as in the previous case, has as its objective a minimal deviation from the original references, as well as the zero-sum constraint. In the following section it will be demonstrated how these objectives can be ensured effectively in a simple manner.

Due to the presented constraints, generated arm currents are not mutually independent. There are in total 6 nodes (ABC and 123), where these currents should sum-up to zero. Nevertheless, five out of six of these constraints are linearly-independent. Therefore, only four out of nine arm current references generated this way are linearly-independent.

To achieve additional energy control actions, power components $P_{\Delta 2}$, $P_{\Delta 3}$, and $P_{\Delta 4}$ from (13) should be considered. Depending on the operating conditions of the converter different scenarios are possible. In the following analysis an example of an M3C feeding a synchronous machine from a 3PH ac grid is used, without loss of generality.

A. SCENARIO I-USING THE LOAD VOLTAGES

In case when the load voltages are available, e.g. a synchronous machine is operating, using the load voltages for additional energy control actions seems to be the best choice. The main reason for this is the fact that the high load voltages would require relatively low additional arm current component. In addition, injection of the common-mode voltages for the purpose of energy control, while the load voltages are present, would necessitate higher voltage/energy reserve in the arms. For those reasons, usage of the load voltages is beneficial, whenever possible.

To perform additional energy control actions using the load voltages, arms connected to the same grid terminals are grouped into bundles, as illustrated in Fig. 2.e. Similarly as before, total power requirement of a bundle is calculated as:

$$P_{x} = \Delta P_{x1} + \Delta P_{x2} + \Delta P_{x3} \qquad (17)$$

These power references are satisfied by introducing the arm current components at load frequency, as shown in (18). Due to the symmetry of the load voltages, thus generated currents do sum-up to zero at the grid terminals.

$$\delta i_{xy} = \frac{2P_{x}}{3\hat{V}_{y}^{2}} v_{y} \qquad (18)$$

Nevertheless, generated current references should also satisfy the zero-sum constraint at the load terminals. Therefore, a modification of the references should be performed, as illustrated in Fig. 2.f. Arms are regrouped into those connected to the same load terminals, and the modification to the references obtained by (18) is performed.

Finally, the total arm current reference is obtained when the three current components are summed together with the load current reference.

$$i_{xy}^{\text{tot}} = i_{xy}^{(\omega_{g})} + \Delta i_{xy}^{**} + \delta i_{xy}^{*} + i_{y}^{*}/3 \qquad (19)$$

Thus generated reference is passed to the arm current controller, whose implementation is not covered in this paper.

B. SCENARIO II-USING THE COMMON-MODE VOLTAGE

Arm energy control has to be performed even in case when the converter is in idling mode, i.e. connected to the grid, but not generating any voltage across its load terminals. In such a case, another scenario should be applied instead of injecting the load-frequency arm current components. The only possibility, according to (13), is injection of the common-mode voltage v_{comm} either at the grid, or at the load frequency. In the first case, common-mode voltage can interact with the existing grid currents, that are covering the converter losses, and thus provide the energy control functionality. In the latter case, additional load-frequency arm currents would have to be generated. While one can opt for any of the two possibilities, the authors of the paper opted for the first one, due to its simplicity.

Under both balanced and unbalanced grid conditions, grid currents are equally distributed among the arms connected to the respective phase. Therefore, as in the case of energy control using the load voltages, a bundle of arms connected to the same grid terminal will be considered as a unit (c.f. Fig. 2.f). Therefore, to produce the required power reference of a bundle, common-mode voltage in-phase with the grid current of the respective terminal should be injected:

$$v_{\text{comm}}^{(x)} = \frac{P_{x}}{|P_{A}| + |P_{B}| + |P_{C}|} \frac{i_{x}}{\hat{I}_{x}} \hat{V}_{\text{comm}} \qquad (20)$$

The amplitude of the common-mode voltage $\hat{V}_{\text{comm}}$ is determined depending on the available voltage reserve, and it case when the load voltage is not generated, it can be as high as the load voltage amplitude.

Three bundles of arms will have different power requirements, and it is necessary to align the common mode voltage with the current of the phase with the highest power requirements. Therefore, the total common-mode voltage injected is determined as:

$$v_{\text{comm}} = v_{\text{comm}}^{(A)} + v_{\text{comm}}^{(B)} + v_{\text{comm}}^{(C)} \qquad (21)$$

To summarize, in case when the load voltage is available, energy control is achieved by setting the arm current reference as in (19). Otherwise, the arm current reference is deprived of the term δi_{xy}^{*}, whereas the common-mode voltage, defined by (20) and (21), is introduced. Therefore, the switch-over between the two control scenarios is easily achieved in the control algorithm.

IV. CURRENT MODIFICATION AND APPLICATION TO THE M3C

To control the arm energies without influencing the grid or load currents, it is necessary to modify the additional arm current components so that they sum-up to zero at corresponding nodes. This was illustrated in Fig. 2.c, where additional arm currents Δi_{A1}, Δi_{B1}, and Δi_{C1} do not generally sum-up to zero, and their sum would appear in the load (terminal 1). Graphical representation of such a case is presented in Fig. 3.a, where phasors of the grid voltages, as well as the additional arm current components are shown. It is obvious
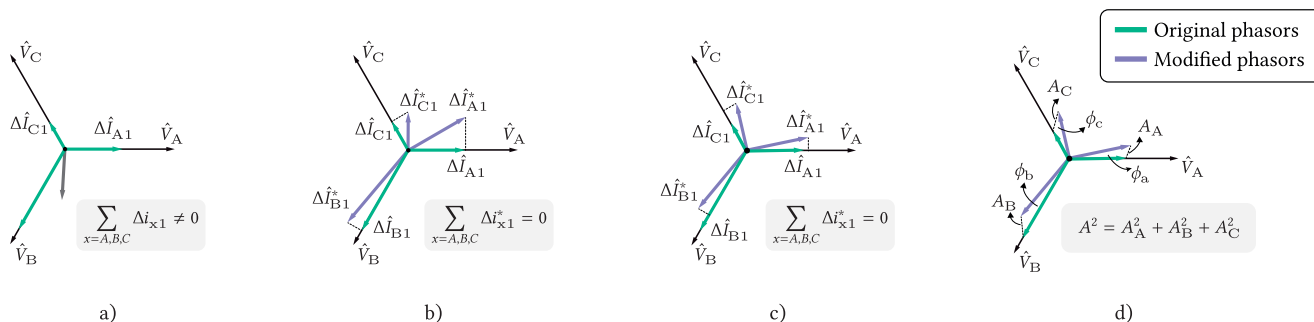
FIGURE 3. Modification of the original set of current references: a) Original set of arm current references; b) Modification of current references that preserves the active power references; c) Modification of current references with the lowest deviation from the original set of currents; d) Criterion used for obtaining the modified set of references.

that due to different power requests from energy controllers, references of the additional arm currents do not sum-up to zero, which imposes the need for their modification.

Similar issue occurs in a standard MMC, and has already been analysed in [10], [11], [27], [28], and [29]. Reference [28] shows two possible approaches in modifying the original current references, illustrated in Fig. 3.b and Fig. 3.c. The first approach modifies the original set of references so that the active power references are preserved, while the zero-sum constraint is ensured. The second approach (c.f. Fig. 3.c) does not preserve the active power references, however it represents the solution that has the minimal deviation with respect to the original references, under the zero-sum constraint. Consequently, this solution yields the modified current references with the lowest magnitude, and with the lowest deviation from the original ones. Fig. 3.d illustrates the function A^2 used as a measure of deviation. The solution in Fig. 3.c is obtained under the zero-sum constraint and minimizing the function A^2. Although the solution does not fully preserve the power references, it is characterized by a simpler implementation with respect to the first one, as well as validity under both balanced and unbalanced grid conditions, as demonstrated in [27].

Fig. 4 shows the implementation of the current modification block. Namely, it can be seen that the new set of references is obtained when the average value of the three currents is subtracted from each one of the initial references. In such a way, modified set of references is the best possible approximation of the initial set under the zero-sum constraint [28]. Therefore, this current modification will be used in all the cases where the zero-sum constraint is present.
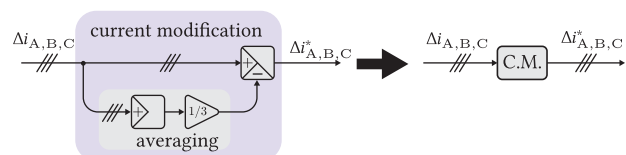
FIGURE 4. Structure of the current references modification block.

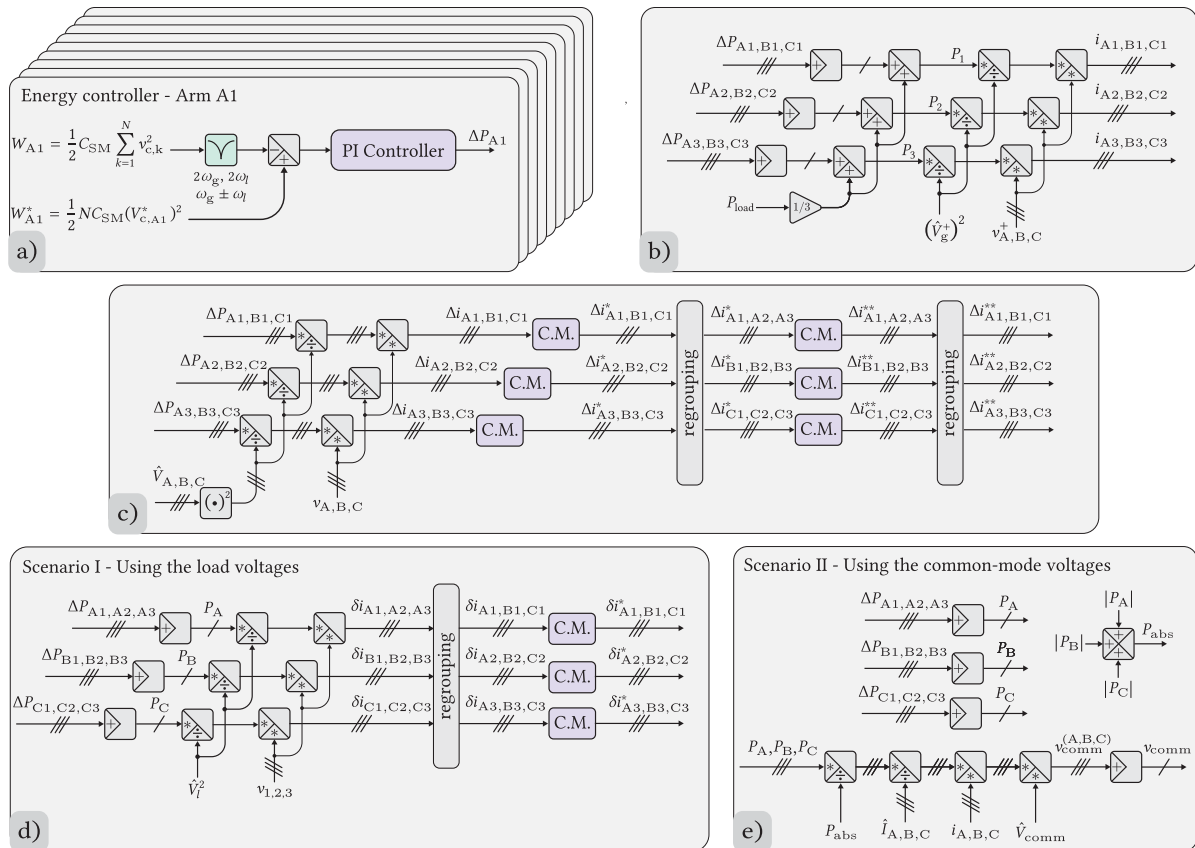Implementation of the arm energy control of the M3C is shown in Fig. 5. Arm energies are calculated from the measured voltages of SMs within an arm, and energy pulsations at specific frequencies are filtered out. The measured value is compared with the energy reference of the respective arm and the error is fed to a PI controller that outputs the power reference ΔP_{xy}, as shown in Fig. 5.a.

The next control action is the control of energies of the bundles of arms connected to the same load terminals. It is based on (14) and (15), and its implementation is shown in Fig. 5.b. The output of this control action are symmetrical arm current references that would make-up the grid current.

Implementation of the internal energy control action, i.e. the one based on interaction of the grid voltage components and additional arm currents that are not observed at the converter terminals, is illustrated in Fig. 5.c. It can be seen that it only contains simple current-modification blocks and regrouping of the references.

The final control action depends on the operating mode of the converter. In this paper, an M3C is assumed to feed a 3PH synchronous machine, which can have three distinctive operating modes: standby mode, generator mode, and motor mode. In case of either motor or generator mode, the voltage at the machine terminals is available, and can be used for energy control, as discussed in the previous section. This mode of converter operation in terms of energy control is referred to as *Scenario I*, and its implementation is illustrated in Fig. 5.d. In case when the machine is in standby mode (not operating), or at very low speed and thus low voltage, a solution using the common-mode voltage is preferable. In this case, the common-mode voltage component is adjusted in terms of its phase and amplitude to interact the most with a grid current of a bundle that has the highest power reference (refer to Fig. 2.e). This mode of operation in terms of energy control is referred to as *Scenario II*, and is illustrated in Fig. 5.e.

While different transitions between the two scenarios might be adopted, the authors of this paper have opted for the simplest one. Namely, for operating modes where the load voltage was higher than half of its rated value, the Scenario I for energy control was used, otherwise it was Scenario II. As it will be demonstrated later, hard switch between the two didn't cause any problem in the converter control.

FIGURE 5. Implementation of the arm energy control of an M3C: a) nine PI energy controllers for nine arms of the converter; b) implementation of the control action that manages the power distribution among the arm bundles connected to the same load terminals; c) generation of the additional arm current components Δi_{xy} and their modification to remain internal to the converter; d) Scenario I of the additional energy control action- generation of the load-frequency additional arm current components δi_{xy}, and their modification to remain unobserved at the converter terminals; e) Scenario II of the additional energy control action - generation of the common-mode voltage at grid frequency.

As described by (19), in case of Scenario I the current references obtained from Fig. 5.b, c and d are summed-up and fed to the arm current controllers. In case of Scenario II, the common-mode voltage reference is created, whereas the current references δi_{xy}^* from Fig. 5.d are not used in the total current reference.

V. REAL-TIME HIL SIMULATOR DESCRIPTION

To facilitate the development of control concepts for the MMC, a real-time (RT) HIL simulator was developed within the laboratory, described in [30]. The control platform used in the MMC and RT HIL is based on ABB's AC 800PEC family of controllers, which aim at performing the top-level MMC control tasks, such as converter pre-charging, control of terminal voltages and currents, energy control, exchanging references and measurements with the SM, etc.

Converter SMs inside the HIL simulator are realized in a hybrid manner. Namely, control part of the SMs are realized by the so-called *Control cards*, shown in Fig. 6, where the local SMs controller is implemented, based on TI TMS320F28069 digital signal processor (DSP). Control cards also host the communication interface between the SM

controller and the top-level control. Power parts of the SMs, i.e. IGBTs, gate-drivers, DC capacitor, are modelled within a Plexim RT-Box 1, and there are in total eight SMs modelled within a single RT-Box. Control cards are interfaced to an RT-Box through the interface board, whereas they are communicating with the top-level controller (AC 800PEC) using the fibre-optic interface. Such a structure represents a single arm of the converter, and is referred to as *Arm unit* in Fig. 6. There are in total nine such units, each one modelling an arm. Due to the same communication interface and the same software running on the DSP of a control card, as it would in the real SM, it is achieved that there is no difference between the HIL-modelled arm and an arm in the real converter, from the perspective of the top-level controller.

Grid and load side of the converter, as well as the interconnections between the arms are modelled using a separate RT-Box and interface board, labelled as *Application unit* in Fig. 6. Thereby, all the power stages of the converter are modelled in the RT HIL simulator, whereas the control hardware corresponds to the one found in the real converter. Consequently, top-level control methods, as well as the SM-level control (implemented on DSPs), can be safely developed
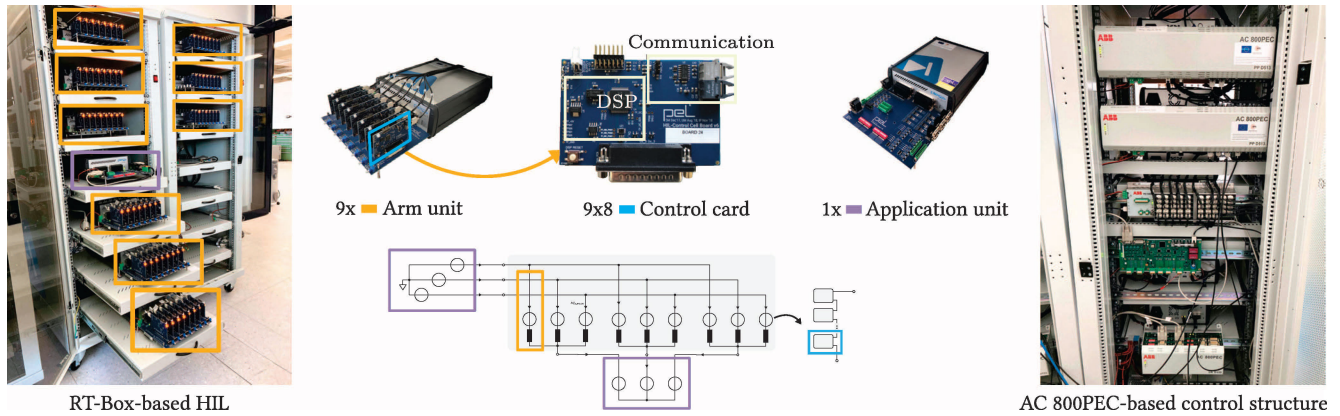
FIGURE 6. Structure of the HIL system modelling the M3C. RT-Box-based HIL consists of 9 arm units, and one application unit. Each arm unit contains N=8 control cards, corresponding to eight SM within an arm. AC 800PEC control structure is as the main control hardware of the converter.
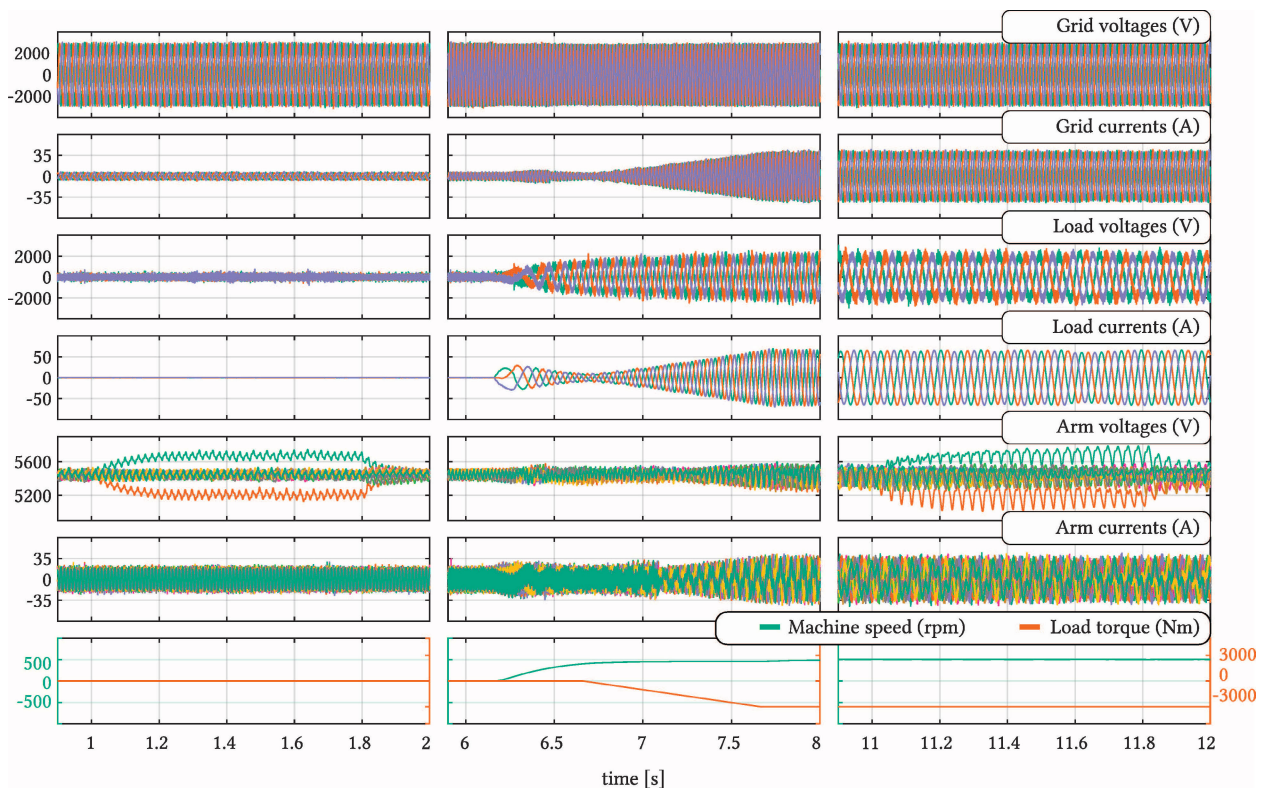
FIGURE 7. Results obtained from the RT HIL simulator. The leftmost plot shows relevant variables of the converter and the machine in standby mode. Energy references of two arms are changed from the rated to demonstrate the effectiveness of the control principle in this mode. The middle plot shows the performance of the converter during dynamic conditions, i.e. machine speed-up and load torque increase. The rightmost plot demonstrates the performance of the energy control method in presence of the load voltage.

and tested using such a system, without making difference between the real converter and the HIL system.

Even though the HIL simulator is not the exact replica of the real converter, it can be considered as a valid platform for control verification. Namely, control hardware and software on both converter and SM level are identical in the HIL simulator and real converter. Modelling of the power stages of the converter in the RT-Box, models all the effects relevant for the current control, energy control and converter operation.

Possible deviations with respect to the actual converter can be expected in unmodelled dynamics of the power switches, deviations of the SM capacitances and arm inductance. However, none of these effects can have a profound influence on the energy control.

VI. REAL-TIME HIL RESULTS AND EVALUATION

Presented control concept was tested on the real-time (RT) HIL simulator, modelling the M3C converter which interfaces
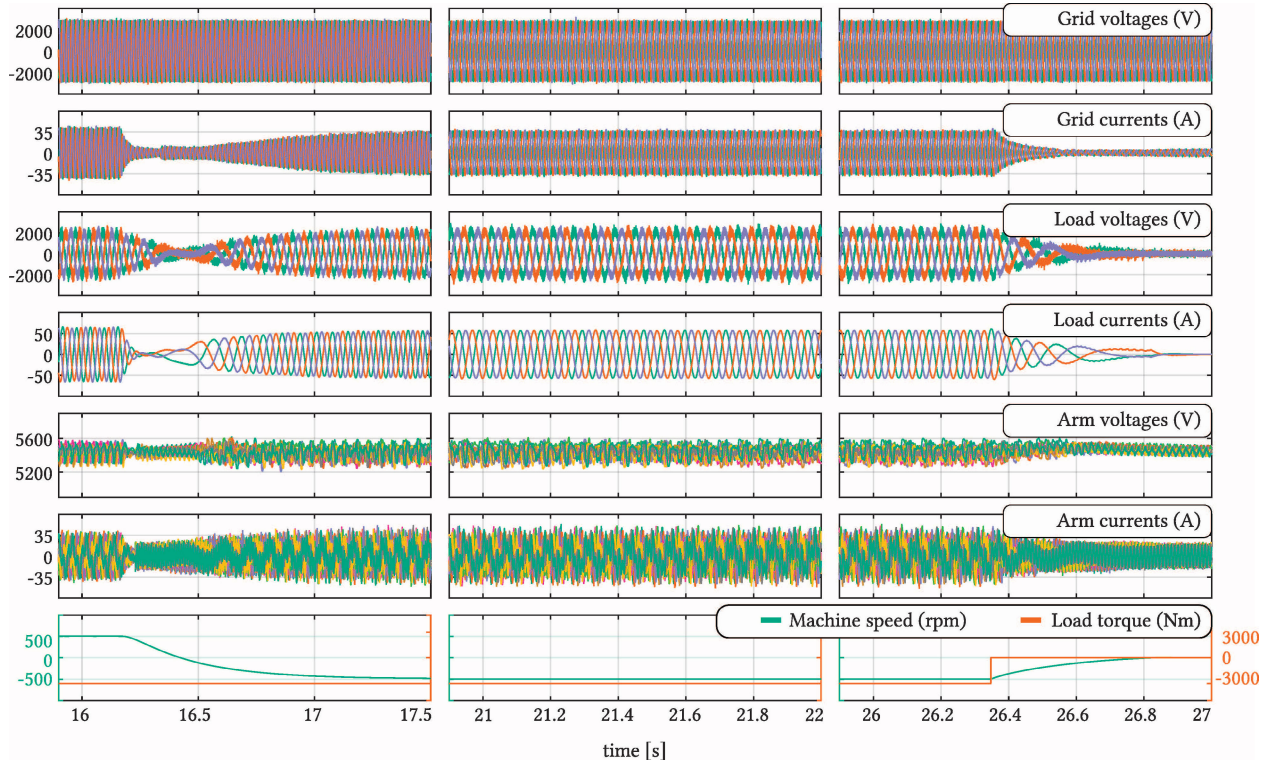
FIGURE 8. Results obtained from the RT HIL simulator. The leftmost plot shows performance of the energy control method during the speed reversal of the synchronous machine. Even though the energy control changes between Scenario I to Scenario II, and back to Scenario I, the arm voltages remain unaffected and follow their reference. The middle plot demonstrates the effectiveness of the control principle in the generator mode of operation. The rightmost plot shows that despite sudden de-loading, followed by machine slowing-down, effectiveness of the energy control is not compromised.

TABLE 1. Converter and machine parameters.

Parameter	Label	Value
Rated grid voltage	V_g^{nom}	3.3 kV
Grid frequency	f_g	50 Hz
Converter rated power	S_{nom}	250 kVA
Number of SM per arm	N_{SM}	8
Rated SM voltage	V_c^*	680 V
SM capacitance	C_{SM}	2.25 mF
Arm inductance	L_{arm}	2.5 mH
IGBT switching frequency	f_{sw}	1 kHz
Machine rated voltage	V_m^{nom}	2.1 kV
Machine rated power	S_m^{nom}	170 kVA
Machine pole pairs	p_m	2
Machine rated speed	n_{nom}	500 rpm
Machine rated torque	T_{nom}	3000 Nm

a medium-voltage grid, and a synchronous machine, as a typical use case of the M3C [6], [31]. Parameters of the grid, converter and machine are provided in Table 1.

The first test scenario is such that the machine is in the standby mode, i.e. at zero speed. Regardless of the fact that the machine is not operating, the converter should be synchronized to the grid, and control its arm energy content. Leftmost part of Fig. 7 shows that the converter maintains the arm voltages around predefined value during this operating mode. In addition, at $t = 1.12$ s voltage references of the SMs in two arms are modified from $V_c^* = 680$ V to $V_c^* = 710$ V and $V_c^* = 650$ V, and set back to the original reference at

$t = 2$ s. In both cases the voltage references are attained within $\Delta t = 200$ ms.

The next scenario is shown as the middle plot of Fig. 7. It represents the machine speed-up to the rated speed, starting at $t = 6.2$ s, and load torque rising to the rated value, starting at $t = 6.7$ s. It can be observed that the arm voltages remain constant throughout the whole transition process, which verifies good performance of the presented control method.

The rightmost plot in Fig. 7 shows converter operation at the rated speed and rated load torque. As in the first test scenario, voltage references of two arms were changed, and energy control was able to ensure reference tracking.

Fig. 8 demonstrates converter's capability to control its energy content under different dynamic conditions, namely during the speed reversal (leftmost plot), negative speed of the machine (middle plot), as well as during the machine de-loading and slowing down.

It is important to notice from Fig. 7 and Fig. 8 that the grid and load currents remain unaffected by the energy control actions, as well as that the transition between different operating modes of the machine, and thus between the two energy control scenarios, remains seamless.

Finally, to verify the performance of the presented control method under unbalanced grid conditions, single-phase-to-ground fault in the grid is simulated during both the standby
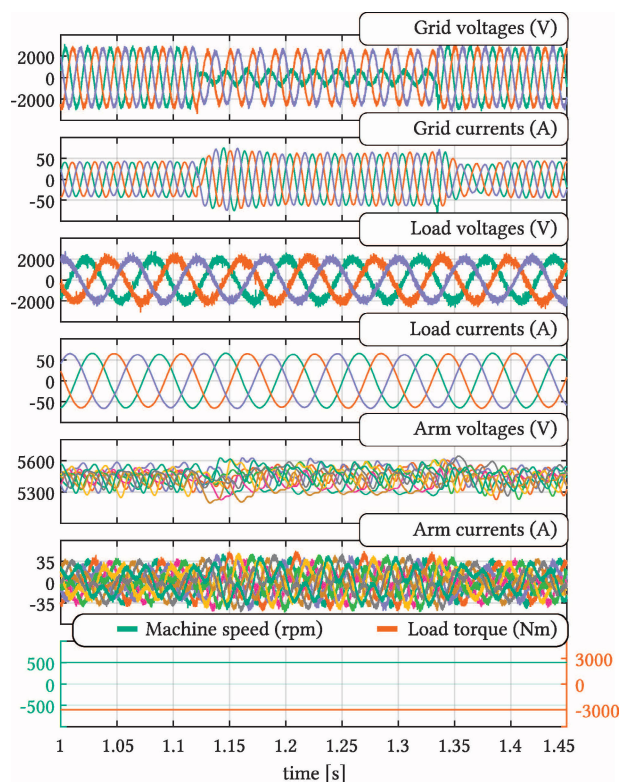
FIGURE 9. Performance verification of the energy control under unbalanced grid conditions. Synchronous machine is in the motor mode of operation, so the energy control is achieved using the load voltages - Scenario I.

FIGURE 10. Performance verification of the energy control under unbalanced grid conditions. Synchronous machine is in the standby mode, so the energy control is achieved using the common-mode voltages- Scenario II.
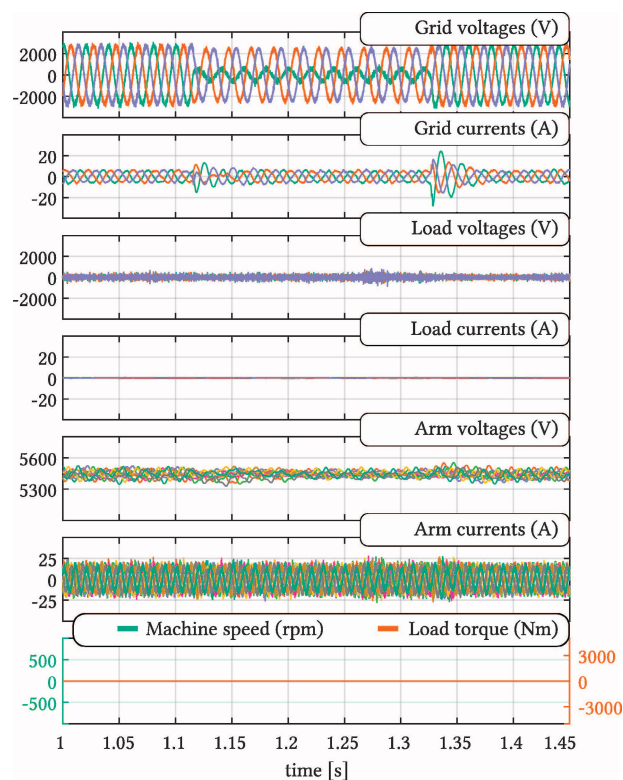
mode of operation (c.f. Fig. 10), and the motor mode of operation of the machine (c.f. Fig. 9). In both cases, arm voltages remained unaffected, thus demonstrating the capability of the two control scenarios to properly work under unbalanced grid conditions.

VII. DISCUSSION

Presented results verify effectiveness of the proposed energy control method, under different imbalances, speed (frequency) reversal, grid unbalanced conditions, as well as under no-load operation. Compared to the methods based on double $\alpha\beta0$ transformations, implementation of the method if far simpler, using only the real-time values of the grid and load quantities, without $\alpha\beta0$ and dq transformations.

Compared to the solution proposed by [18], bulky matrices with real-time variable elements are omitted, whereas the transition between the low-frequency (low load voltage) and high-frequency operating modes can be seamlessly performed. Additionally, the proposed solution was verified under unbalanced grid conditions, even under the combined unbalance and no-load conditions, in contrast to [18].

Comparing the solution against its rival in terms of simplicity [22], the solution in [22] cannot ensure an arbitrary energy control under normal conditions, neither can it

ensure decoupling of the internal balancing currents from the terminal currents under grid faults. Therefore, although the solution [22] seems as the simplest one, it in fact does not perform well under all operating modes.

A detailed comparison between the balancing performance of the methods mentioned above, including the here introduced direct arm control balancing method, can be found in [32]. The authors conducted a theoretical comparison as well as real-time HIL tests to establish the characteristics of each method. The evaluated aspects include the dynamic response, degrees of freedom, low-voltage ride-through performance as well as the mathematical simplicity and the implementation simplicity.

One might argue that the proposed solution does not preserve all the power references yielded by the energy controllers, due to the current modification blocks. While this claim is true, the current modification block is optimized so as to minimize the circulating currents imposed in the converter arms, while still ensuring the energy balancing under all conditions.

Finally, simplicity of implementation, coupled with the fact that the current modification is optimized to reduce the current stress on the converter while ensuring an arbitrary energy control, make this solution unique, simple to understand and implement, and robust for various operating modes.

VIII. CONCLUSION

This paper presents extension of the direct arm energy control method, firstly derived for the standard MMC, to the M3C. The energy control method presented in this paper is derived using an intuitive approach, resulting in a simple implementation, which might be of great value to control engineers and researchers entering the field. Besides ensuring that the energy control actions are not observed at the converter terminals, presented control method proves to be valid under different operating conditions of a synchronous machine, as well during transients. It was demonstrated that the arm energies can be arbitrarily controlled, and that the control method is equally applicable under balanced and unbalanced grid conditions.

REFERENCES

[1] R. W. Erickson and O. A. Al-Naseem, "A new family of matrix converters," in *Proc. 27th Annu. Conf. IEEE Ind. Electron. Soc.*, vol. 2, Nov. 2001, pp. 1515–1520.

[2] A. Lesnicar and R. Marquardt, "An innovative modular multilevel converter topology suitable for a wide power range," in *Proc. IEEE Bologna Power Tech Conf.*, vol. 3, Jun. 2003, pp. 1–6.

[3] D. Weiss, M. Vasiladiotis, C. Banceanu, N. Drack, B. Odegard, and A. Grondona, "IGCT based modular multilevel converter for an AC–AC rail power supply," in *Proc. Int. Exhib. Conf. Power Electron., Intell. Motion, Renew. Energy Energy Manag.*, May 2017, pp. 1–8.

[4] M. Winkelnkemper, A. Korn, and P. Steimer, "A modular direct converter for transformerless rail interties," in *Proc. IEEE Int. Symp. Ind. Electron. (ISIE)*, Jul. 2010, pp. 562–567.

[5] Y. Okazaki, W. Kawamura, M. Hagiwara, H. Akagi, T. Ishida, M. Tsukakoshi, and R. Nakamura, "Experimental comparisons between modular multilevel DSCC inverters and TSBC converters for medium-voltage motor drives," *IEEE Trans. Power Electron.*, vol. 32, no. 3, pp. 1805–1817, May 2017.

[6] M. Vasiladiotis, R. Baumann, C. Haderli, and J. Steinke, "IGCT-based direct AC/AC modular multilevel converters for pumped hydro storage plants," in *Proc. IEEE Energy Convers. Congr. Expo. (ECCE)*, Sep. 2018, pp. 4837–4844.

[7] M. Hagiwara, R. Maeda, and H. Akagi, "Control and analysis of the modular multilevel cascade converter based on double-star chopper-cells (MMCC-DSCC)," *IEEE Trans. Power Electron.*, vol. 26, no. 6, pp. 1649–1658, Jun. 2011.

[8] K. Ilves, L. Harnefors, S. Norrga, and H.-P. Nee, "Predictive sorting algorithm for modular multilevel converters minimizing the spread in the submodule capacitor voltages," *IEEE Trans. Power Electron.*, vol. 30, no. 1, pp. 440–449, Jan. 2015.

[9] S. Fan, K. Zhang, J. Xiong, and Y. Xue, "An improved control system for modular multilevel converters with new modulation strategy and voltage balancing control," *IEEE Trans. Power Electron.*, vol. 30, no. 1, pp. 358–371, Jan. 2015.

[10] A. J. Korn, M. Winkelnkemper, P. Steimer, and J. W. Kolar, "Capacitor voltage balancing in modular multilevel converters," in *Proc. 6th IET Int. Conf. Power Electron., Mach. Drives*, Mar. 2012, pp. 1–5.

[11] M. Basic, S. Milovanovic, and D. Dujic, "Comparison of two modular multilevel converter internal energy balancing methods," in *Proc. 20th Int. Symp. Power Electron.*, Oct. 2019, pp. 1–8.

[12] F. Kammerer, J. Kolb, and M. Braun, "A novel cascaded vector control scheme for the modular multilevel matrix converter," in *Proc. 37th Annu. Conf. IEEE Ind. Electron. Soc.*, Nov. 2011, pp. 1097–1102.

[13] F. Kammerer, J. Kolb, and M. Braun, "Fully decoupled current control and energy balancing of the modular multilevel matrix converter," in *Proc. 15th Int. Power Electron. Motion Control Conf. (EPE/PEMC)*, Sep. 2012, pp. LS2a.3-1–LS2a.3-8.

[14] W. Kawamura, M. Hagiwara, and H. Akagi, "Control and experiment of a modular multilevel cascade converter based on triple-star bridge cells," *IEEE Trans. Ind. Appl.*, vol. 50, no. 5, pp. 3536–3548, Sep./Oct. 2014.

[15] F. Kammerer, M. Gommeringer, J. Kolb, and M. Braun, "Energy balancing of the modular multilevel matrix converter based on a new transformed arm power analysis," in *Proc. 16th Eur. Conf. Power Electron. Appl.*, Aug. 2014, pp. 1–10.

[16] M. Diaz, R. Cardenas, M. Espinoza, F. Rojas, A. Mora, J. C. Clare, and P. Wheeler, "Control of wind energy conversion systems based on the modular multilevel matrix converter," *IEEE Trans. Ind. Electron.*, vol. 64, no. 11, pp. 8799–8810, Nov. 2017.

[17] M. Diaz, R. Cardenas, M. Espinoza, C. M. Hackl, F. Rojas, J. C. Clare, and P. Wheeler, "Vector control of a modular multilevel matrix converter operating over the full output-frequency range," *IEEE Trans. Ind. Electron.*, vol. 66, no. 7, pp. 5102–5114, Jul. 2019.

[18] D. Karwatzki and A. Mertens, "Generalized control approach for a class of modular multilevel converter topologies," *IEEE Trans. Power Electron.*, vol. 33, no. 4, pp. 2888–2900, Apr. 2018.

[19] B. Fan, K. Wang, P. Wheeler, C. Gu, and Y. Li, "An optimal full frequency control strategy for the modular multilevel matrix converter based on predictive control," *IEEE Trans. Power Electron.*, vol. 33, no. 8, pp. 6608–6621, Aug. 2018.

[20] M. Urrutia, R. Cardenas, J. Clare, M. Diaz, and A. Watson, "Continuous set model predictive control for energy management of modular multilevel matrix converters," *IEEE Trans. Power Electron.*, vol. 37, no. 5, pp. 5731–5748, May 2022.

[21] M. Urrutia, R. Cardenas, J. C. Clare, and A. Watson, "Circulating current control for the modular multilevel matrix converter based on model predictive control," *IEEE J. Emerg. Sel. Topics Power Electron.*, vol. 9, no. 5, pp. 6069–6085, Oct. 2021.

[22] J. Ma, M. S. A. Dahidah, V. Pickert, and J. Yu, "A hierarchical energy balance control method for M³C based on injecting output frequency circulating currents," *IEEE Trans. Power Electron.*, vol. 35, no. 3, pp. 2424–2435, Mar. 2020.

[23] A. J. Korn, M. Winkelnkemper, P. Steimer, and J. W. Kolar, "Direct modular multi-level converter for gearless low-speed drives," in *Proc. 14th Eur. Conf. Power Electron. Appl.*, 2011, pp. 1–7.

[24] W. Kawamura, Y. Chiba, M. Hagiwara, and H. Akagi, "Experimental verification of an electrical drive fed by a modular multilevel TSBC converter when the motor frequency gets closer or equal to the supply frequency," *IEEE Trans. Ind. Appl.*, vol. 53, no. 3, pp. 2297–2306, May/Jun. 2017.

[25] B. Fan, K. Wang, P. Wheeler, C. Gu, and Y. Li, "A branch current reallocation based energy balancing strategy for the modular multilevel matrix converter operating around equal frequency," *IEEE Trans. Power Electron.*, vol. 33, no. 2, pp. 1105–1117, Feb. 2018.

[26] K. Ilves, L. Bessegato, and S. Norrga, "Comparison of cascaded multilevel converter topologies for AC/AC conversion," in *Proc. Int. Power Electron. Conf.*, May 2014, pp. 1087–1094.

[27] M. Utvic and D. Dujic, "Direct arm energy control in modular multilevel converter under unbalanced grid conditions," in *Proc. Int. Symp. Power Electron., Electr. Drives, Autom. Motion (SPEEDAM)*, Jun. 2020, pp. 250–256.

[28] M. Utvić and E. P. F. de Lausanne, "Generalized theory on direct arm energy control in modular multilevel converters," *CPSS Trans. Power Electron. Appl.*, vol. 5, no. 4, pp. 388–399, Dec. 2020.

[29] P. Münch, D. Görges, M. Izak, and S. Liu, "Integrated current control, energy control and energy balancing of modular multilevel converters," in *Proc. 36th Annu. Conf. IEEE Ind. Electron. Soc. (IECON)*, Nov. 2010, pp. 150–155.

[30] S. Milovanovic, I. Polanco, M. Utvic, and D. Dujic, "Flexible and efficient MMC digital twin realized with small-scale real-time simulators," *IEEE Power Electron. Mag.*, vol. 8, no. 2, pp. 24–33, Jun. 2021.

[31] P. Bontemps, N. Hugo, and D. Dujic, "Flexibility enhancements in pumped hydro storage power plants through variable speed drives," in *Proc. 46th Annu. Conf. IEEE Ind. Electron. Soc.*, Oct. 2020, pp. 1820–1825.

[32] P. Bontemps, S. Milovanovic, and D. Dujic, "Performance analysis of energy balancing methods for matrix modular multilevel converters," *IEEE Trans. Power Electron.*, vol. 38, no. 3, pp. 2910–2924, Mar. 2023.

MILAN UTVIĆ (Graduate Student Member, IEEE) received the B.Sc. and M.Sc. degrees from the School of Electrical Engineering, University of Belgrade, Serbia, in 2015 and 2017, respectively. He is currently pursuing the Ph.D. degree with the Power Electronics Laboratory, École Polytechnique Fédérale de Lausanne (EPFL), Switzerland. From 2016 to 2017, he worked as a Research Assistant with the Department of Power Converters and Drive Systems, University of Belgrade. From February 2018 to February 2022, he was with the Power Electronics Laboratory, EPFL. From April to June 2020, he was with the ABB Traction Department, Turgi, Switzerland, as an industrial Ph.D. internship. Since February 2022, he has been employed as a Power Electronics Engineer at H55 SA, working on electric propulsion systems for all electric aircraft. His research interests include utility scale high power converters, power converters for renewables, electric drives, and traction power converters.

PHILIPPE BONTEMPS (Graduate Student Member, IEEE) received the B.Sc. and M.Sc. degrees from the École Polytechnique Fédérale de Lausanne (EPFL), Lausanne, Switzerland, in 2017 and 2019, respectively, where he is currently pursuing the Ph.D. degree.

In 2019, he joined the Power Electronics Laboratory, EPFL, as a Doctoral Research Assistant. His research interest includes multilevel conversion systems for high-power medium-voltage applications.

DRAŽEN DUJIĆ (Senior Member, IEEE) received the Dipl.-Ing. and M.Sc. degrees in electrical engineering from the University of Novi Sad, Novi Sad, Serbia, in 2002 and 2005, respectively, and the Ph.D. degree in electrical engineering from Liverpool John Moores University, Liverpool, U.K., in 2008.

From 2002 to 2006, he was with the Department of Electrical Engineering, University of Novi Sad, as a Research Assistant. From 2006 to 2009, he was with Liverpool John Moores University, as a Research Associate. From 2009 to 2013, he was with the ABB Corporate Research Centre, Switzerland, as the Principal Scientist, working on the power electronics projects spanning the range from low-voltage/power SMPS in below kilowatt range to medium voltage high-power converters in a megawatt range. From 2010 to 2011, he was a member of a project team responsible for the development of the world's first power electronic traction transformer successfully commissioned on the locomotive. From 2013 to 2014, he was with ABB Medium Voltage Drives, Turgi, Switzerland, as a Research and Development Platform Manager, responsible for ABB's largest IGCT-based medium voltage drive ACS6000. He is currently with the École Polytechnique Fédérale de Lausanne (EPFL), Lausanne, Switzerland, as an Associate Professor and the Director of the Power Electronics Laboratory. He has authored or coauthored more than 200 scientific publications and has filed 20 patents. His current research interests include the areas of design and control of advanced high-power electronics systems for medium voltage applications.

Dr. Dujić has received the First Prize Paper Award from the Electric Machines Committee of the IEEE Industrial Electronics Society, in 2007. In 2014, he has received the Isao Takahashi Power Electronics Award for outstanding achievement in power electronics, and in 2018, the EPE Outstanding Service Award from the European Power Electronics and Drives Association. He is an Associate Editor of the IEEE Transactions on Power Electronics.

• • •